Preliminary Findings on the Correlation between Left Atrial Wall Shear Stress and Atrial Endocardial Voltage in Atrial Fibrillation

Camilla Cortesi[1,2], Matteo Falanga[2], Jonas Leite[1], Shannon Soulez[1], Nadjia Kachenoura[1], Cristiana Corsi[2]

[1] Sorbonne Université, CNRS, INSERM, Laboratoire d'Imagerie Biomédicale, LIB, Paris, France
[2] DEI, University of Bologna, Campus of Cesena, Bologna, Italy

Abstract

Left atrial (LA) wall fibrosis plays a significant role in atrial fibrillation (AF) due to atypical electrophysiological characteristics of such tissue substrate. However, the mechanism underlying the development of such fibrosis is poorly understood.

The purpose of this preliminary study was to investigate the possible association between LA wall shear stress (WSS), assessed using computational fluid dynamics (CFD), and areas with fibrosis, defined by low values of bipolar voltage (BV<0.5 mV). Simulations were run on patient-specific dynamic LA models derived from MRI and CT data of 10 AF patients. The focus of the analysis was to assess the impact of the computational model on the distribution of fluid dynamic parameters and the association between LA WSS and endocardial voltage.

Our preliminary findings suggest that the computational domain affects CFD simulation results, with more consistent findings for the MRI-derived than for the CT-derived model.

1. Introduction

Atrial fibrillation (AF) is associated with structural remodelling of the left atrial (LA) chamber, which consequently leads to modifications in circulating blood and hemodynamic, contributing to an increased risk of thrombus development and stroke [1]. Additionally, AF is associated with the development of LA fibrosis, which is considered as a tissue substrate of arrhythmia.

Wall shear stress (WSS), defined as the frictional force per unit area exerted by the tangential component of blood flow on the wall, has been recognized as a major hemodynamic factor. It has been associated with function, geometry, and tissue composition in various cardiovascular vessels, including the aorta and the coronary arteries [2].

Computational fluid dynamics (CFD) allows for the assessment of LA and left atrial appendage (LAA) flow on a vastly improved spatial and temporal scale compared to current non-invasive 4D flow MRI. This enables an accurate assessment of shear stresses in the LA and LAA. Previously, CFD-derived low and oscillatory shear conditions were linked to thrombosis in AF[3, 4]. These patient-specific models may be used to predict stroke and characterize pro-thrombotic hemodynamic circumstances after a sufficient validation in larger clinical cohorts [5, 6].

During electrophysiological procedures, LA bipolar voltage (BV) is a frequently utilized measure to identify the presence of fibrotic tissue in atrial myocardium. The presence of low voltage regions has been associated with arrhythmia recurrence after AF ablation, persistent forms of AF, and has recently been used as a tool to define targets for ablation [7].

In this preliminary study, we investigate the possible association between CFD-derived LA WSS and areas with fibrosis, defined by low values of BV (<0.5 mV), in patients with AF, while comparing both MRI and CT-derived patient-specific anatomical models.

2. Materials and Methods

2.1. Patients Data

This study was a retrospective analysis of 10 patients with AF, imaged whilst in sinus rhythm from the CTStrain-AF Study (NCT04281329), an observational study conducted by Assistance Publique-Hôpitaux de Paris (AP-HP) and approved by the institutional review board.

The participants, who had AF and were all over 18 years, were scheduled for their first radiofrequency ablation, an interventional treatment for AF, within the next six months, and provided written informed consent for their participation. Pre-ablation imaging was performed at the Centre Hospitalier Universitaire Pitié-Salpêtrière, Paris, including routine computed tomography (CT) and research cardiac MRI exam (Sola, 1.5T, Siemens Healthineers) with 4D flow acquisition. 4D flow MRI consists of an anatomical reference volumetric acquisition encompassing the LA throughout the cardiac cycle and the corresponding X, Y, and Z velocity components.

4D flow MRI images were reconstructed in 25 time frames (pixel size 2.375 mm², slice thickness 3 mm).

CT data were reconstructed in 11 or 21 time frames (pixel size 0.4-0.5 mm², slice thickness 0.6 mm).

The 3D electro-anatomical map of the LA, consisting of its complete anatomy and the BV map, was acquired for each patient right before the AF ablation procedure.

2.2. Data Analysis

The workflow for the analysis of 4D flow MRI and CT data is summarized in Figure 1 and includes several steps that are described in the next section.

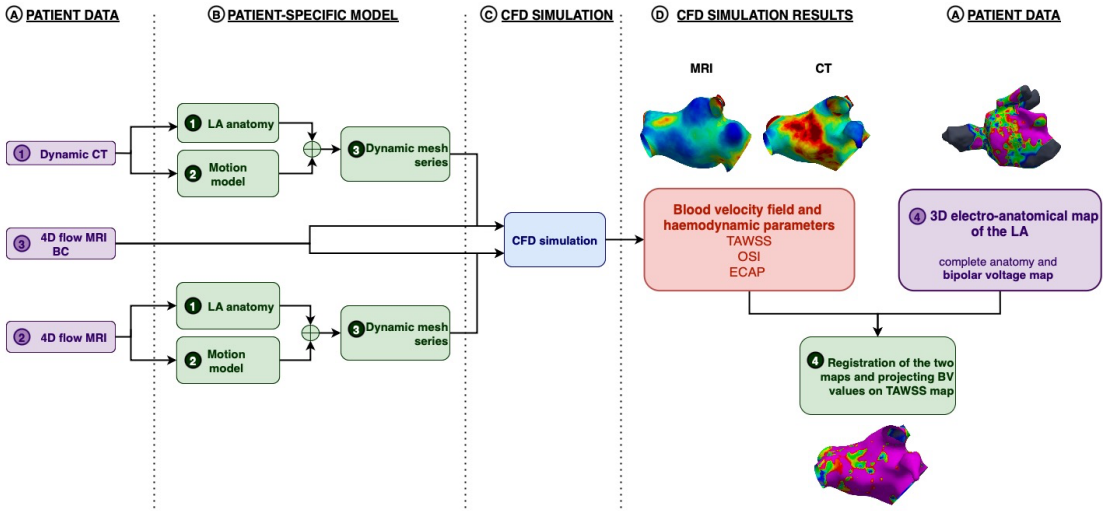

Figure 1: Workflow of the study: patient-specific CT (A1) and 4D flow MRI (A2) data are processed to derive the LA anatomical and displacement models (B1-2) from which a dynamic model (B3) is computed; the latter represents the computational domain for the personalized CFD model (C) using PVs flowrate from 4D flow MRI as boundary conditions (A3). The results of the CFD simulations are evaluated in terms of blood velocity field and hemodynamic parameters: Time-Averaged Wall Shear Stress (TAWSS), Oscillatory Shear Index (OSI), Endothelial Cell Activation Potential (ECAP) (D) and registered with the 3D electro-anatomical map (A4) to get a unique map with both hemodynamic parameters and voltage values projected on it (B4).

The 4D flow anatomical volume corresponding the ventricular end-diastole was manually segmented using ITK-SNAP (version 3.8.0, Kitware Inc.) to extract the 3D LA anatomical model.

CT volume corresponding the ventricular end-diastole was segmented by applying a pre-trained 3D U-net and then manually corrected if needed.

For both 4D flow MRI and CT, volume registration and initial mesh propagation were performed using Elastix [4] to obtain the patient-specific displacement model. The Transformix library was then used to apply the transformation matrix in order to register the reference volume on the remaining time frames. A B-spline model performed the non-rigid registration, optimized using the mean squared difference. Both 4D flow MRI-derived dynamic model and CT-derived dynamic model were supplied as input to a customized CFD model [8] to run fluid-dynamic simulations in sinus rhythm conditions.

The use of the incompressible Navier-Stokes equations in the Arbitrary Lagrangian Eulerian frame of reference [9] allowed for the replication of blood flow as a fluid.

Patient-specific boundary conditions (BCs), in terms of pulmonary veins (PVs) flowrate, were extracted from 4D flow MRI and applied to the CFD simulations. To extract the velocity profiles at the PVs, a semi-automated approach was applied. First, the best fitting plane was computed considering the PVs ostium barycentre and its normal vector. Afterwards, the volume of interest (VOI) corresponding to the PVs trunks was extracted by intersecting the mesh nodes and faces with the best-fitting plane. Finally, the 3D velocity field modulus from 4D flow MRI was interpolated within the mesh vertices at the PVs.

In addition, to take into account the size of each PV, we applied the mass balance equation as follows:

$$Q_{LIPV} + Q_{LSPV} + Q_{RIPV} + Q_{RSPV} + Q_0 + Q_{wall} = 0$$

$$Q_{wall} = \frac{dV}{dt}$$

where Q_{LIPV}, Q_{LSPV}, Q_{RIPV}, Q_{RSPV} are the flowrate at the left inferior, left superior, right inferior, and right superior PV, respectively, Q_0 is the flowrate at the MV, and Q_{wall} is the flow related to LA volume variation. Each flowrate was calculated as $Q_{\mathrm{PV}} = v_{\mathrm{PV}} A_{\mathrm{PV}}$, where v_{PV} indicates the velocity values and A_{PV} indicates the PVs cross-sectional area.

The dynamic viscosity was adjusted to 0.035 poise, the density to 1.06 g/cm^3, and the time step to 0.001 seconds. The LifeX package was used to run the simulations [10].

In order to mitigate the impact of the initial fluid velocity conditions on the results, we conducted a simulation with three heartbeats and solely examined the final one.

Blood velocity field and several common hemodynamic metrics used in the assessment of thrombosis were derived: 1) time-averaged wall shear stress (TAWSS), representing the integration of the WSS vector magnitude over the cardiac cycle; 2) oscillatory shear index (OSI), describes the WSS vector's departure from its average direction; 3) ECAP, which is defined as OSI/TAWSS.

The 3D electro-anatomical map of the LA was registered to the hemodynamic map in 2 steps, comprising a rigid registration and an iterative closest point (ICP) registration. Finally, the BV values were mapped on the hemodynamic map anatomy to allow a direct comparison.

An automatic approach was applied to perform the LA regionalization [11,12] and divide it into 6 well-defined anatomical regions (Figure 3B), to locally evaluate the associations between TAWSS and BV values.

3. Results and Discussion

Patient characteristics and LA and LAA haemodynamic data are summarized respectively in Table 1 and Table 2, revealing a clear difference between the LA mean normalized end-diastolic volume extracted from CT and MRI. This difference reflected the large difference between the spatial resolution of the two modalities and was mainly visible in the LAA. Indeed, LAA complex anatomy was highly detailed in the CT-derived model, while its structure was missing in detail and precision in the MRI-derived model.

	Mean	SD
Sex (male/female)	5/5	-
Age [yrs]	66.4	5.6
Weight [kg]	81.6	14.6
Height [cm]	169.9	8.7
BSA [m²]	1.9	0.2
CT Indexed LA Vol [mL/m²]	62.5	14.1
MRI Indexed LA Vol [mL/m²]	49.2	13.7
LA BV [mV]	1.9	0.6

Table 1: Patient baseline characteristics. BSA = body surface area, SD = standard deviation.

		CT		MRI	
		Mean	SD	Mean	SD
LA:	TAWSS [Pa]	0.28	0.05	0.20	0.05
	OSI	0.19	0.02	0.18	0.04
	ECAP [/Pa]	0.95	0.16	1.54	0.78
LAA:	TAWSS [Pa]	0.12	0.05	0.06	0.04
	OSI	0.29	0.06	0.25	0.09
	ECAP [/Pa]	6.76	4.93	9.38	8.33

Table 2 (below): Hemodynamic data in the LA and LAA comparing the CT-derived model and MRI-derived model. TAWSS = time-averaged wall shear stress, OSI = oscillatory shear index, ECAP = endothelial cell activation potential.

A significant difference in terms of TAWSS emerged from the comparison between CT and MRI-derived results in the LA ($p = 0.0002$) and LAA ($p = 0.023$), both in the distribution and localisation of the values (Figure 2), resulting in higher TAWSS for the CT-derived model, as compared to the MRI-derived model.

There was no significant difference between CT and MRI-derived models in terms of average values when examining OSI.

A significant difference between CT and MRI emerged in the LA chamber ECAP mean value ($p = 0.029$), while it was not significant in the LAA. Despite the anatomical differences, in both CT- and MRI-models, the site characterized by the highest rate of thrombogenic risk is the LAA.

Both CT and MRI normalized LA volume presented a negative correlation with TAWSS, as expected due to physiological behaviour; however, such correlation was significant only for MRI ($p = 0.010$). MRI-derived OSI had a positive correlation with the LA volume, although this did not reach statistical significance. Such expected positive association was not found for the CT-derived OSI. Finally, for both CT and MRI-derived models, ECAP showed a positive correlation with the LA volume, as expected, and such correlation was significant for MRI ($p = 0.009$) but not for CT.

In line with the aforementioned results, the correlation between the percentage of low voltage area (LVA) and the hemodynamic parameters in CT- and MRI-derived models reflected the patterns observed for

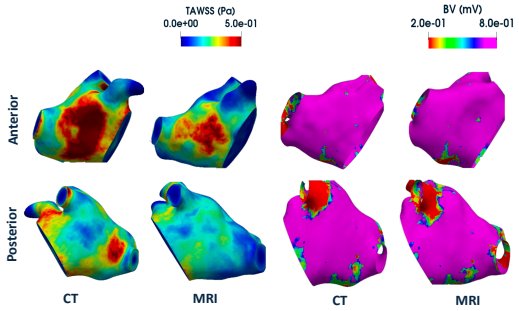

Figure 2: anterior and posterior views of CT-derived and MRI-derived TAWSS and BV map of an example patient.

LA volume. Notably, within the MRI-derived model, LVA exhibited statistically significant associations with both TAWSS ($p = 0.046$) and ECAP ($p = 0.002$), whereas these relationships did not reach statistical significance in the CT-derived model.

These preliminary results suggest that the computational domain affects the simulation results, and the image modality chosen for the anatomical model should be taken into consideration among the other variables. Despite most of the studies in the literature being based on models derived from CT imaging [3-6], in this conducted investigation, the results from MRI appear to better reproduce the fluid dynamics of the LA. It should be noted that the BCs applied to the simulations were derived directly from 4D flow MRI. Overall, despite the major limitation of the spatial resolution of 4D flow MRI, the LA fluid dynamics seem to be better replicated by the MRI-derived model.

We had also investigated the possible correlation of TAWSS with LVA on the LA wall at the local level (Figure 3A). The disparity between the CT-derived model and the MRI-derived model resulted in different distribution of TAWSS values. At the regional level, the TAWSS values in the CT model were higher in both LVA and no LVA, confirming what has been shown for the entire LA chamber. In the inferior, septal, anterior, and LAA areas, for both CT- and MRI-derived models, lower BV values correspond to lower TAWSS values. While for the lateral and posterior region the distribution of TAWSS values was more homogeneous between the CT- and MRI-derived models.

These preliminary results are in line with Paliwal et al. findings, where a CFD model was applied to a group of 8 AF patients, revealing lower TAWSS in fibrotic regions [13]. In their study, hemodynamic characteristics of the LA were compared against spatial mapping of myocardial fibrosis assessed using late gadolinium enhancement MRI to investigate potential local and global relationships.

This study opens up several improvements. Future work should confirm these findings in a broader cohort. The amount of fibrosis in our patients was relatively low, indicating an early stage of AF-induced remodelling. Imaging data were acquired with the patient in sinus rhythm. This constrains the generalizability of the findings to patients with persistent AF, who may demonstrate a distinct interaction between hemodynamics and BV.

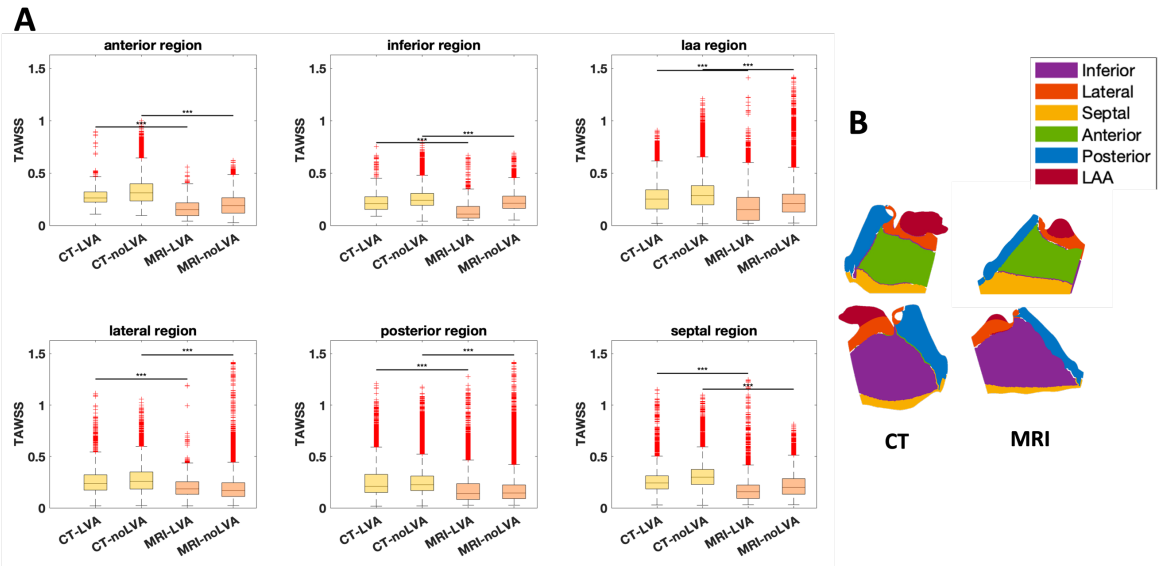

Figure 3: (A) Box plots showing the distribution of TAWSS values across six atrial regions (anterior, inferior, LAA, lateral, posterior, and septal) for CT and MRI low voltage area (LVA- BV < 0.5 mV) and no low voltage area (noLVA – BV ≥ 0.5mV). Significant differences across imaging modalities are indicated (*p < 0.05, **p < 0.01, ***p < 0.001). (B) Representative CT- and MRI-derived LA geometries with regional segmentation (inferior, lateral, septal, anterior, posterior, and LAA regions shown in distinct colours).

4. Conclusions

This work employs patient-specific CFD simulations derived from non-invasive imaging data to evaluate potential correlations between fibrosis and blood flow hemodynamic in the LA of AF patients. The difference in spatial and temporal resolution between imaging data used to derive anatomical models affects the simulation results. The results from the MRI-derived model appear to better reproduce the fluid dynamics of the LA compared to the CT-derived model.

On a local level, there was evidence that regions of low voltage values correlate with lower TAWSS. These results suggest that the fibrotic region in the LA of AF patients might lead to abnormal hemodynamic conditions, which could lead to thrombogenesis near these areas, potentially causing stroke.

References

[1] Wolf, P.A., et al.: Atrial fibrillation as an independent risk factor for stroke: the Framingham Study. Stroke 22, 983–988 (1991). https://doi.org/10.1161/01.str.22.8.983

[2] Chatzizisis, Y. S. et al.: Role of endothelial shear stress in the natural history of coronary atherosclerosis and vascular remodeling: molecular, cellular, and vascular behavior. J. Am. Coll. Cardiol. 49, 2379–2393 (2007).

[3] Parker, L., et al.: A multi-modal computational fluid dynamics model of left atrial fibrillation haemodynamic validated with 4D flow MRI (2024). https://doi.org/10.21203/rs.3.rs-4606278/v1

[4] Bosi, G.M., et al.: Computational fluid dynamic analysis of the left atrial appendage to predict thrombosis risk (2018). https://doi.org/10.3389/fcvm.2018.00034

[5] Falanga, M., et al.: A digital twin approach for stroke risk assessment in atrial fibrillation patients. Heliyon. 10, e39527 (2024). https://doi.org/10.1016/j.heliyon.2024.e39527

[6] Dueñas-Pamplona, J., et al.: A comprehensive comparison of various patient-specific CFD models of the left atrium for atrial fibrillation patients. Comput. Biol. Med. 133, 104423 (2021). https://doi.org/10.1016/j.compbiomed.2021.104423

[7] Williams SE, et al.: The effect of activation rate on left atrial bipolar voltage in patients with paroxysmal atrial fibrillation. J Cardiovasc Electrophysiol 2017;28:1028–36.

[8] Masci, A., et al.: A Proof of concept for computational fluid dynamic analysis of the left atrium in atrial fibrillation on a patient-specific basis. J Biomech Eng. vol. 142(1):011002, Jan 2020.

[9] Hirt, C.W., et al.: An arbitrary Lagrangian-Eulerian computing method for all flow speeds, J. Comput. Phys., Volume 14, Issue 3, 1974, Pages 227-253, ISSN 0021-9991, https://doi.org/10.1016/0021-9991(74)90051-5.

[10] Africa, P.C.: "Lifex: a flexible, high performance library for the numerical solution of complex finite element problems", SoftwareX 20, 101252 (2022).

[11] Althoff, Till F., et al.,: Regionalization of the atria for 3D electroanatomical mapping, cardiac imaging, and computational modelling: a clinical consensus statement of the European Heart Rhythm Association and the European Association of Cardiovascular Imaging of the ESC, EP Europace, Volume 27, Issue 7, July 2025, euaf134

[12] Hussain, S., et al.,: Patient-specific left atrium contraction quantification associated with atrial fibrillation: A region-based approach, CMPB, Volume 249 2024, 108138, ISSN 0169-2607, https://doi.org/10.1016/j.cmpb.2024.108138.

[13] Paliwal, N., et al. (2021): Presence of left atrial fibrosis may contribute to aberrant hemodynamics and increased risk of stroke in atrial fibrillation patients. Front. Physiol. 12:657452. doi: 10.3389/fphys.2021.657452

Address for correspondence:

Camilla Cortesi
Via dell'Università 50, 40057 Cesena (FC), Italy
camilla.cortesi@etu.sorbonne-universite.fr
camilla.cortesi3@unibo.it